CrossMark

RESEARCH ARTICLE

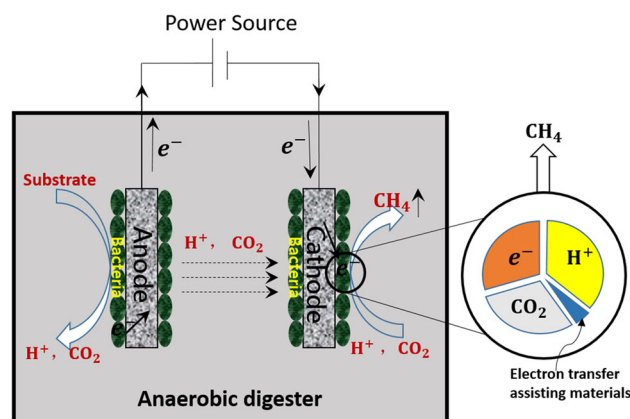# Decoration of graphite fiber fabric cathode with electron transfer assisting material for enhanced bioelectrochemical methane production

Qing Feng[1] · Young-Chae Song[1]

Abstract The surface of graphite fiber fabric (GFF) was mounted with an electron transfer assisting material, such as Ni, Fe, or ammonia, along with multiwall carbon nanotube (MWCNT) to enhance the growth of electrochemically active bacteria (EAB) using an electrophoretic deposition method. The decorated surface of GFF was changed to rough and porous, and the electric conductivity was improved from 7.52 to less than $0.2\ \Omega\ cm^{-1}$. The bioelectrochemical methane productions for the decorated cathodes were compared in a batch bioelectrochemical anaerobic reactor. During the enrichment of EAB on the cathode, it was observed that the decorated cathode requires a longer initial lag phase (9–23 days), but the maximum methane production rate from the control cathode is considerably improved after the enrichment of EAB. The decoration materials reduce the charge transfer resistance on the cathode for the bioelectrochemical reduction of carbon dioxide, and improve the production of methane. The effectiveness of the electron transfer assisting materials for the bioelectrochemical methane production was in the order of Ni, Fe, and ammonia. The maximum methane production rate for the cathode decorated with MWCNT and Ni was $44.8\ mL\ CH_4\ L^{-1}\ d^{-1}$, which was 57.2 % higher than the control GFF cathode, and the methane yield was as much as $326.3\ mL\ CH_4\ g^-COD_r^{-1}$ compared to the $252.8\ mL\ CH_4\ g^-COD_r^{-1}$ for the control cathode, or $162.1\ mL\ CH_4\ g^-COD_r^{-1}$ of the anaerobic control.

Graphical abstract Schematic diagram of electron transfer assisting material on the cathode for enhancing bioelectrochemical methane production.

1 Introduction

Anaerobic digestion has been recognized as a popular green technology to stabilize organic waste while recovering renewable energy as biogas. However, anaerobic digestion is being investigated as a viable method in the hope of improving some of its limitations, such as a low organic matter degradation rate, long retention time, poor effluent quality, low purity of biogas, as well as, the troubles that arise in the operation of the process [1, 2]. These limitations are mainly caused by the slow hydrolysis rate of particulate organic matter, slow growth rate of methanogens, and susceptibility of methanogens to environmental

✉ Young-Chae Song
soyc@kmou.ac.kr

1 Department of Environmental Engineering, Korea Maritime and Ocean University, Busan 606-791, South Korea

changes [1, 3]. Recently, an innovative approach has been developed, in which the anaerobic digestion system was coupled with Bioelectrochemical technology to mitigate the limitations in the anaerobic digestion. [2, 4–11]. In the coupled anaerobic digestion, methane is produced from electrochemically active bacteria (EAB) on the electrode surface, as well as planktonic anaerobic bacteria (PAB) in liquid phase. In the case of methane production from EAB, organic matter is oxidized by some of EAB attached on the anode surface and produces protons, carbon dioxide, and electrons [2, 4, 12]. The protons and carbon dioxide are released into the solution, while the electrons are transferred to the anode, and then moved to the cathode through an external electrical circuit. At the surface of cathode, methane is bioelectrochemically formed by the reduction of carbon dioxide combined with electrons and protons [2, 4, 6, 11]. For the bioelectrochemical methane production, the electric potential of the cathode is poised to overcome the thermodynamic barrier [2, 11]. Then, the bioelectrochemical reaction on the cathode is catalyzed by methanogenic species of EAB growing on the cathode. The methanogenic species and their biomass on the cathode surface during the enrichment of EAB are affected by the physical and electrochemical properties of the electrode, such as roughness, surface area, electric conductivity, and electric potential [13–18]. In particular, the electrochemical properties of the cathode materials are an important factor that influences the catalytic activity of EAB on the cathode. However, available information on the cathode materials is still not adequate. It is well known that several carbon-based materials, such as carbon cloth, carbon felt, and carbon fiber, are biocompatible, durable in chemical solution, and reasonable in price. Among them, some porous carbon materials in the form of felt and fabric have wide surface area available for bacterial growth, and recommended as good raw materials for cathode [19–22]. The porous carbon materials, however, are generally insufficient in the electric conductivity and catalytic activity for the electrochemical reduction on cathode. The surface of porous carbon materials could be physico-chemically and electrochemically modified with catalytic materials assisting electron transfer for a better performed cathode [17, 23, 24]. Multiwall carbon nanotube (MWCNT) is a material with highly conductive and wide surface area, and it is frequently adopted as a supporter for catalytic materials [25, 26]. Up to date, several substances, including cobalt tetramethylphenylporphyrin (CoTMPP), iron phthalocyanine (FePC), manganese oxide (MnO$_x$), ammonia (NH$_3$), nickel (Ni), and platinum (Pt), have been examined as catalytic materials in bioelectrochemical systems [21, 22, 27–29]. Although Pt was always the best as the catalyst for the reductions on cathode, it

was too expensive to use in the field scale [26, 30]. In recent, the reduction of carbon dioxide into methane on the cathode was successfully improved by some non-precious metals, such as nickel, copper, and iron, as well as the nitrogen doping material using ammonia treatment [31–35]. These imply that the porous carbon materials could be modified to a good cathode for bioelectrochemical methane production by surface decoration using the above materials.

In this study, three different cathodes were prepared by decorating with three catalytic materials (Ni, Fe, and ammonia) together with MWCNT on the surface of Graphite fiber fabric (GFF), and the bioelectrochemical methane production from the cathodes was examined in batch anaerobic reactor.

2 Materials and methods

2.1 Electrode preparation

GFF (Samjung C&G Co., Korea) and multiwall carbon nanotube (MWCNT, Carbon Nano-material Technology Co., Ltd., Korea) were submerged in concentrated nitric acid for 24 h to remove impurities, and then washed with running tap water. Different electrolyte solutions were prepared by mixing 1.0 g MWCNT, 0.5 g polyethylenimine, and one of the electron transfer assisting materials including 0.25 g of NiCl$_2$, FePC, and NH$_3$Cl with 1 L of distilled water. The MWCNT and assisting materials were simultaneously loaded on each surface of the GFF by electrophoretic deposition (EPD) method at 30 V for 30 min, and three different cathodes, hereafter referred to as Ni–C, Fe–C, and Am–C, were obtained. The GFF without any treatment, referred to as GFF-C, was prepared as a control cathode. For the anode, the MWCNT and the Ni were loaded on the GFF surface by EPD method using the same procedure for the Ni–C preparation. A paste of EG (exfoliated graphite) and MWCNT was screen-printed to form a scaffold layer on the GFF surface, and then hot pressed for 15 min at 200 °C to complete the anode. For the EG, an acidified graphite powder soaked with diluted sulfuric acid and chromic acid (Hyundai Coma Industry, Inc., Korea) was exfoliated using microwave radiation for 10 s, and then reduced using Hydrazine solution as in a previous study [17]. The paste of EG and MWCNT was obtained by mixing 1 g of MWCNT, 1 g of EG, 100 mL of ethanol, and 10 mL of binder. The binder was prepared by dissolving 2 g of coal tar pitch into 10 mL of toluene. The anode and cathode were submerged into a sodium dodecyl sulfate (SDS) solution (1 %) to improve the hydrophilicity before use according to a previous study [18].

2.2 Batch bioelectrochemical reactor for methane production

A single chamber glass bottle with 0.75 L of effective volume was used for batch bioelectrochemical anaerobic reactor (Fig. 1). A separator and electrode assembly (SEA) was prepared by stacking, in the following order: the anode, separator, and cathode, and then rolled into a cylindrical shape (6.2 cm dia., 8 cm height). A commercial non-woven polypropylene sheet was used as the separator. The SEA was installed in the bottle reactor, and each electrode was connected to an external circuit with titanium wires. Seed sludge (0.23 L) and substrate medium (0.52 L) were added to the reactor. The seed sludge was taken from an anaerobic digester for sewage sludge (S sewage treatment plant, Busan, Korea). The substrate medium consisting of 3 g L^{-1} glucose, 2.45 g L^{-1} NaH_2PO_4, 4.58 g L^{-1} Na_2HPO_4, 0.31 g L^{-1} NH_4Cl, 0.31 g L^{-1} KCl, 10 mL L^{-1} vitamins, and 5 mL L^{-1} trace minerals was prepared according to a previous study [18, 36]. The top of the bottle reactor was covered with a plastic cap for air sealing. On the plastic cap, two ports for biogas outlet and biogas sampling were installed, respectively. The biogas outlet port was connected to a floating gas collector with a rubber tube, and the gas collector was filled with an acidic solution that was saturated with sodium chloride to prevent biogas resolution. The biogas sampling port was covered with an *n*-butyl rubber stopper. The potential difference between the anode and the cathode was controlled to be 0.3 V using an external DC power supply [2, 12, 37], and then stirred with a magnetic bar at 300 rpm. The bioelectrochemical reactor was incubated in a constant temperature room controlled at

Fig. 1 Schematic diagram of a batch bioelectrochemical anaerobic reactor

35 ± 1 °C. As a control, an anaerobic batch reactor without electrodes was also incubated at same conditions as the bioelectrochemical reactors. During incubation, biogas production was monitored using the gas collector, and the substrate medium was replaced with a fresh one when it was depleted. The first cycle of the batch operation was done for the enrichment of EAB, and then four more cycles of the batch operation were continued to estimate the bioelectrochemical methane production from different cathodes.

2.3 Analysis and calculations

The precise surface features of the cathodes were obtained using a scanning electron microscope (SEM, MIRA-3, Tescan, Czech), and the elemental compositions of the cathode surfaces were analyzed by energy dispersive X-ray spectroscopy (EDS) based on the SEM. The resistance of the cathodes was measured by a Hall Effect measurement system (HMS-3000, Ecopia Co., Korea). In order to confirm the substrate consumption, chemical oxygen demand (COD) was measured at the beginning and end of the batch cycle operation according to Standard Methods (2005). Biogas production was also monitored from the floating type gas collector, and the composition of biogas was analyzed by a gas chromatograph (Series 580, GOW-MAC Instrument Co., USA) equipped with a packed column (Porpak Q 6ft × 1/8 in SS, Restek Co., USA) and a thermal conductivity detector (TCD). Methane production ($V_{CH_4,i}$) at each monitoring time interval was calculated from the measurements of the biogas volume and their methane contents in the headspace of the bottle reactor and the gas collector using the following mass balance equation:

$$V_{CH_4,i} = C_{CH_4,i}\left(V_{G,i} + V_R\right) - V_R C_{CH_4,i-1}. \qquad (1)$$

Here $V_{G,i}$ is the total biogas volume (mL) measured in the gas collector at the current time interval (i), and V_R is the headspace volume of the bottle reactor. $C_{CH_4,i}$ and $C_{CH_4,i-1}$ are the methane fractions in the head space of the reactor measured using gas chromatography in the current and previous time intervals, respectively. Next, the methane production ($V_{CH_4,i}$) was expressed as a standard temperature pressure (STP) state using the following equation:

$$V_{CH_4}(\text{at STP}) = V_{CH_4,i}(\text{at } T) \times \frac{273}{273 + T} \times \frac{760 - W}{760}, \qquad (2)$$

where T is the incubation temperature (35 °C) of the reactor, and W is the water vapor pressure at 35 °C (mmHg). The cumulative methane production for the enrichment stage of EAB was fit to the modified Gompertz equation [38]:
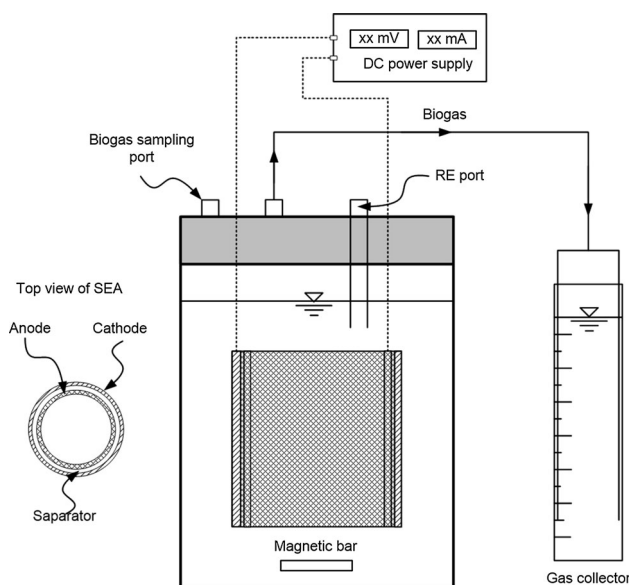
$$P = P_\mathrm{u} \exp\left[-\exp\left(\frac{\mu_\mathrm{m} \cdot \exp(1)}{P}(\lambda - t) + 1 \right) \right]. \tag{3}$$

Here, μ_m represents the maximum methane production rate (mL g-COD^{-1} d^{-1}); λ is the lag phase time (days); and P_u is the ultimate methane production (mL g-COD^{-1}). The average cumulative methane production was calculated from final three batch cycles after the enrichment stage, and then fit to Eq. (3). During the operation of the reactor, the potentials for the anode and the cathode were frequently monitored with a portable digital multimeter (Fluke 87-V, Fluke Co., USA) and Ag/AgCl reference electrode (AlsCo., Ltd., Japan). Electrochemical impedance spectra (EIS) for the cathode were obtained in the frequency band ranging from 100 kHz to 10 MHz with an AC signal amplitude of 25 mV using an electrochemical instrument (CompactStat, Ivium Technologies, The Netherlands). At open circuit condition, the cathode as working electrode and the anode as count electrode were connected to the terminals of electrochemical instrument, and an Ag/AgCl electrode was submerged in the reactor content as a reference electrode. The EIS data were fit to a mixed kinetic and diffusion control model using IviumStat analysis software. The model includes a solution resistance in series with a double-layer capacitor, which is in parallel with the faradic reaction impedance consisting of a charge transfer resistance and Warburg element in series. A linear voltage sweep for the cathode was also conducted in the potential range between −200 and 650 mV (vs. Ag/AgCl reference electrode) with a 10mV s^{-1} scan rate. The polarization data for the cathodes were fit to Eq. (4), and the Tafel slope (β) and exchange current (i_o) were obtained from the extrapolation of the linear region ($r > 0.999$) by

$$E = \alpha + \beta \log i/i_0 \tag{4}$$

where E is the potential ($E_0 + \eta$); α and i are the intercept of the Tafel curve and the anodic current density, respectively; and η and E_0 are the overpotential and the equilibrium potential.

3 Results and discussion

3.1 Morphology of the cathode surfaces

Figure 2 displays SEM images for the cathode surfaces decorated with different materials assisting the electron transfer of EAB. The crystalline aggregations of the materials deposited on the graphite fiber strands appeared on the decorated cathode surfaces, which were porous and rough. The GFF-C without any decoration consisted of clean and smooth strands of carbon fibers. In bioelectrochemical methane production, the reduction of carbon dioxide into methane is catalyzed by the EAB, which is growing on the cathode surface [4, 7, 16]. It is likely that the materials decorated on the cathode surface support the growth of EAB by assisting electron transfer on the cathode, as well as, altering the cathode surface to a more biocompatible and porous structure, which are favorable conditions for bacterial growth [2, 19, 21].

The elemental composition of the cathode surfaces was further examined by EDS (Table 1). The major elemental components of the decorated cathodes were carbon (74.7–87.6 At. %) and oxygen (7.3–20.9 At. %), while a small portion of the assisting materials were also appeared on the cathodes. This indicates that the crystalline aggregations on the cathode surface, the assisting materials, were properly decorated on the cathode surfaces by the EPD method. The percentage of the assisting materials appearing were in the range of 0.5–2.3 At. %, which was varied in the types of the materials. The GFF-C as the control cathode consisted of carbon (89.5 At. %) and oxygen (10.5 At. %).

The electric resistance for the GFF-C was observed as high as 7.52 Ω cm^{-1} (Table 1). The high resistance of the GFF-C was likely due to the contact resistance between the loose bundles of the carbon fiber strands. The electric resistances for the cathodes decorated with the assisting materials were considerably reduced, and in particular, the electric resistance for the Ni–C was 0.07 Ω cm^{-1}, which was slightly lower than the others. The resistance for the Am–C decorated with non-conductive ammonia compound was also low, namely 0.15 Ω cm^{-1}. This indicates that the improved electric conductivities for the decorated cathodes were mainly attributed to the MWCNT, which was loaded on the surface of the carbon fiber strands, and was bridged between the carbon fiber strands. The MWCNT is often used as a conducting bridge for the improvement of electric conductivity for various composites [39, 40].

3.2 Enrichment stage of EAB on the decorated cathodes

The bioelectrochemical methane production during the enrichment stage of EAB on the cathode surface was considerably affected by the decoration materials (Ni, Fe, or ammonia) (Fig. 3). Methane production for the decorated cathodes started to increase slowly after initial lag phases of 9.4–22.5 days, but the lag phases for the GFF-C without any decoration and the anaerobic digestion control were only 13.0 and 6.9 days, respectively (Table 2). The long lag phase in the bioelectrochemical system is due to the time for the initial selection of EAB and adaptation to the new environment before beginning exponential growth [41, 42].The lag phase depends on the seed sludge, the roughness, and biocompatibility of the electrode surface, as well as, electrochemical properties [18, 42]. It seems that
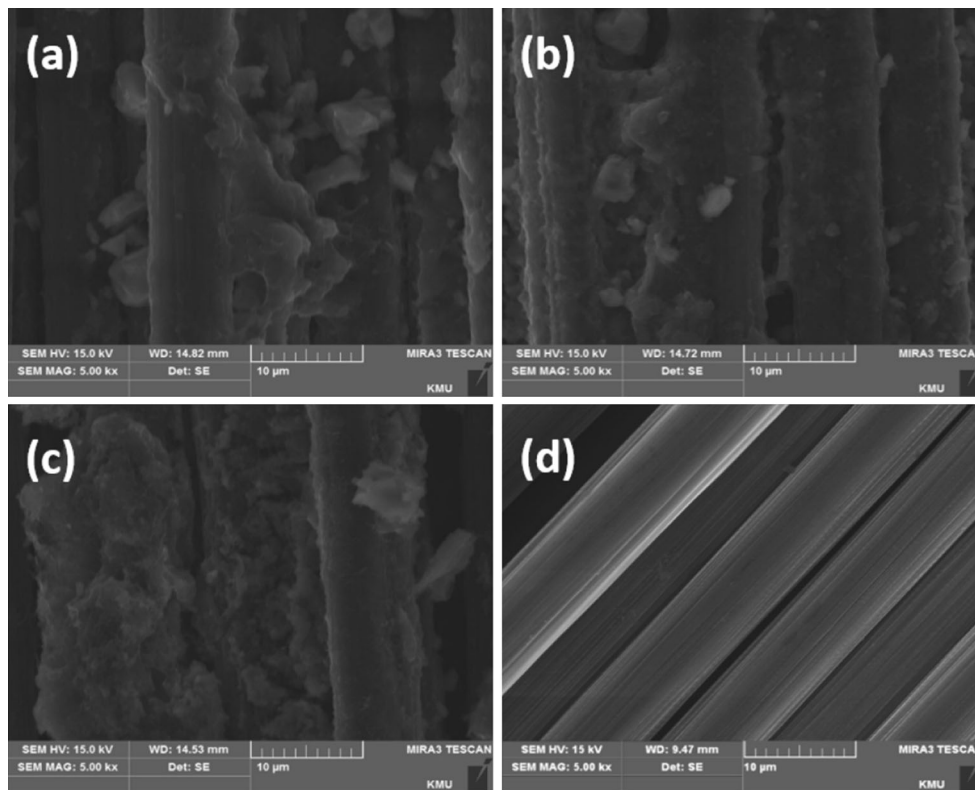
Fig. 2 SEM images for the different cathode surfaces decorated with the materials assisting with the electron transfer: **a** Ni–C, **b** Fe–C, **c** Am–C, and **d** GFF-C

Table 1 Elemental compositions and electrical conductivities for different cathode surfaces

Element (At. %)	Ni–C	Fe–C	Am–C	GFF-C
C (%)	87.6	77.2	74.7	89.5
O (%)	7.3	20.9	14.2	10.5
Cl (%)	2.9	1.4	9.3	
Ni (%)	2.3	–	–	–
Fe (%)	–	0.5	–	–
N (%)	–	–	1.8	–
Resistance (Ω cm^{-1})	0.07	0.19	0.15	7.52

Fig. 3 Cumulative methane productions from the bioelectrochemical reactors with the cathodes decorated with different materials during the enrichment stage of EAB

the initial attachment of bacteria on the electrode surface is affected by the types of seed sludge and the electrode physical properties, such as its roughness and biocompatibility, and the selection and adaption of EAB on the electrode surface depend on the electrochemical properties of the surface. The long lag phases for bioelectrochemical methane production compared to the control are most likely due to the seed sludge taken from an anaerobic digester for sewage sludge. The dominant species in the anaerobic sludge from a conventional anaerobic digester for sewage sludge are not EAB. This indicates that the materials (Ni, Fe, and ammonia) decorated on the cathode
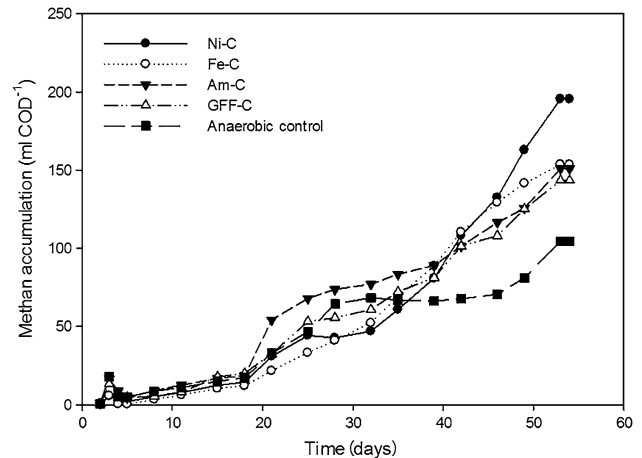
surface do not directly catalyze the electrochemical conversion of carbon dioxide into methane within conditions for mesophilic anaerobic digestion. The lag phase for the Am-C was shorter (9.38 days) than the GFF-C. This suggests that the biocompatibility on the cathode surface is improved by the ammonia treatment. In previous study, the ammonia treatment for the electrode improved bacterial

Table 2 Summary of estimated bioelectrochemical methane production from different cathodes

Parameter	Stage	Ni–C	Fe–C	Am–C	GFF-C	Control
P_u (mL CH$_4$ g-COD^{-1})	E	215.9	163.0	166.0	158.4	114.2
	M	237.3 ± 8.4	176.2 ± 1.9	178.9 ± 6.7	156.8 ± 10.0	89.2 ± 16.6
μ_m (mL CH$_4$ g-COD^{-1} d^{-1})	E	6.2	5.4	3.6	3.7	2.4
	M	44.8 ± 2.4	35.4 ± 1.6	34.0 ± 1.9	28.5 ± 2.3	17.8 ± 3.8
$\lambda(d)$	E	22.51	20.49	9.38	13.01	6.90
	M	0.35 ± 0.15	0.65 ± 0.12	0.89 ± 0.20	1.38 ± 0.34	1.53 ± 0.28
r^2	E	0.975	0.990	0.979	0.985	0.965
	M	0.981 ± 0.002	0.987 ± 0.006	0.991 ± 0.001	0.991 ± 0.005	0.985 ± 0.004
Yield (mL CH$_4$ g-COD$_r^{-1}$)	M	326.3 ± 13.9	235.9 ± 17.9	272.2 ± 20.4	252.8 ± 12.5	162.1 ± 18.9

E EAB enrichment stage, *M* matured stage after the EAB enrichment

attachment on the surface, and then the initial acclimation time of EAB was reduced in MFCs [35]. However, the lag phases for Ni–C and Fe–C were over 20 days, which were considerably longer than 13 days of the lag phase for the GFF-C (Table 2). This suggests that the selection and adaptation of EAB is stricter on the surface that is more electrochemically active, which caused a longer time for enrichment stage but not the inhibitory effects of decorated materials. In previous studies, it took a long enrichment time (10–30 days) of EAB on the surface of electrochemically active electrode after the inoculation of anaerobic sludge for sewage sludge [2, 18, 41, 43].

The maximum methane production rate provides insight into the growth of EAB on the cathode surface. The maximum methane production rate was 6.2 mL CH$_4$ g-COD^{-1} d^{-1} for the Ni–C, and 5.4 mL CH$_4$ g-COD^{-1} d^{-1} for the Fe–C. The maximum methane production rate of the Am–C was 3.6 mL CH$_4$ g-COD^{-1} d^{-1}, and similarly for the GFF-C (3.7 mL CH$_4$ g-COD^{-1} d^{-1}). The methane in the bioelectrochemical anaerobic reactor is a main product from the metabolic process of electrochemically active methanogens. This implies that the growth rate of the methanogens could be inferred from the maximum methane production rate during log growth phase in batch reactor. It seems that the growth rate of EAB is the highest on the Ni–C, followed by the Fe–C, GFF-C, and Am–C, respectively, indicating that the bioelectrochemical metabolic process for methane production depends on the electrochemical properties of the cathode surface.

3.3 Bioelectrochemical methane productions from different cathodes

After the enrichment of EAB on the cathode surface, the influence of the decoration materials on bioelectrochemical methane production was distinct (Fig. 4). The cumulative methane production was quickly increased after a short lag phase when the substrate medium was replaced with a fresh
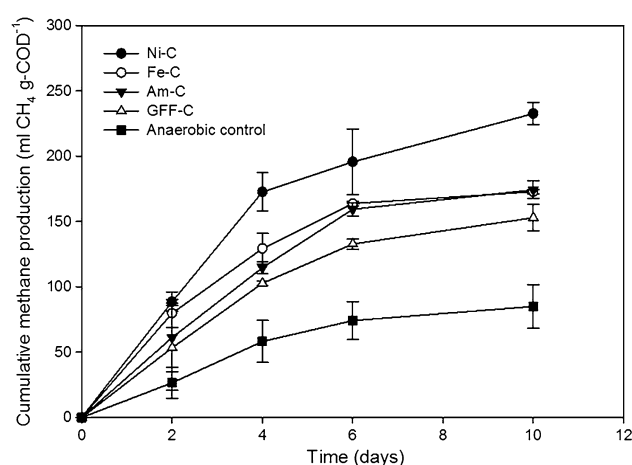

Fig. 4 Cumulative methane productions from the bioelectrochemical reactors with the cathodes decorated with different materials after the enrichment of EAB

one (Table 2). The maximum methane production rate is an indicator of the methanogenic potential of EAB on the cathode, which was obtained from the greatest slope of the cumulative methane production. The maximum methane production rate was 28.5 mL CH$_4$ g-COD^{-1} d^{-1} for GFF-C, which was higher than the value of 17.8 mL CH$_4$ g-COD^{-1} d^{-1} for the anaerobic control (Table 2). This shows that the bioelectrochemical activity for methane production is higher than conventional anaerobic digestion. However, the maximum methane production rate for the Ni–C was considerably higher, namely 44.8 mL CH$_4$ g-COD^{-1} d^{-1}. This result suggests that the bioelectrochemical methanogenic activity was significantly improved by the decoration of Ni and MWCNT on the cathode surface. The maximum methane production rates for the Fe–C and the Am–C were similar to one another, but were less than the Ni–C. It is believed that the bioelectrochemical methanogenic activity is a function of EAB species and their biomass on the cathode surface. The species and

biomass of EAB are possibly affected by the decoration materials assisting the electron transfer of EAB on the cathode surface [44].

The bioelectrochemical methane yield was 326.3 mL CH_4 g-COD_r^{-1} for the Ni–C, which was 29.1 % higher than 252.8 mL CH_4 g-COD_r^{-1} for the GFF-C (Table 2). However, the methane yields were 235 mL CH_4 g-COD_r^{-1} and 272 mL CH_4 g-COD_r^{-1} for both of the Fe–C and the Am–C, respectively, which are also higher than 162.1 mL CH_4 g-COD_r^{-1} for the anaerobic control. The overpotential for bioelectrochemical methane production leads to energy loss in the electrode reaction. The ultimate methane production of the Ni–C is higher than the others, indicating that the energy loss of the Ni–C for the bioelectrochemical conversion of carbon dioxide into methane is less than the others. The applied voltage is distributed to electrodes (anode and cathode) depending on the electrochemical properties of the electrodes during the enrichment stage of EAB. However, the electrode potentials could be considerably changed by the enrichment of EAB on the electrodes. It seems that the electron balance on the anode and cathode determines the distribution of applied voltage to the electrodes [2, 12, 18].

3.4 Electrochemical properties of the decorated cathodes

The results of the EIS experiments for the decorated cathodes are fit well by a Randles equivalent circuit model in the Nyquist representation (Fig. 5a). This suggests that the reduction of carbon dioxide into methane was mainly controlled by charge transfer, and partly by diffusion on the cathode surface. However, the semi-circles were a little flat, and the centers were below the real axis. The incomplete flat semi-circle is commonly observed as the current is not uniform on the cathode due to the inhomogeneous electrode surface [45, 46]. The estimated values of charge transfer resistance (R_{ct}), capacitance (C), Warburg (W) for the cathodes decorated with the electron transfer assisting materials are presented in Table 3. The solution ohmic resistances (R_S) for the cathodes were in the range of 1.24–1.33 Ω, which was similar to the GFF-C (1.27 Ω). The semi-circle diameter of the Nyquist plots is the charge transfer resistance. The charge transfer resistances were 3.1 Ω for the Ni–C, which was lower than those for the Fe–C or the Am–C. The charge transfer resistance for the GFF-C was 8.6 Ω. The activation energy is described by a function of the charge transfer resistance on the cathode surface using the Arrhenius equation [47, 48]. The small charge transfer resistance suggests that the cathode has a kinetic advantage for bioelectrochemical methane production, indicating that Ni is a better decoration material assisting the electron
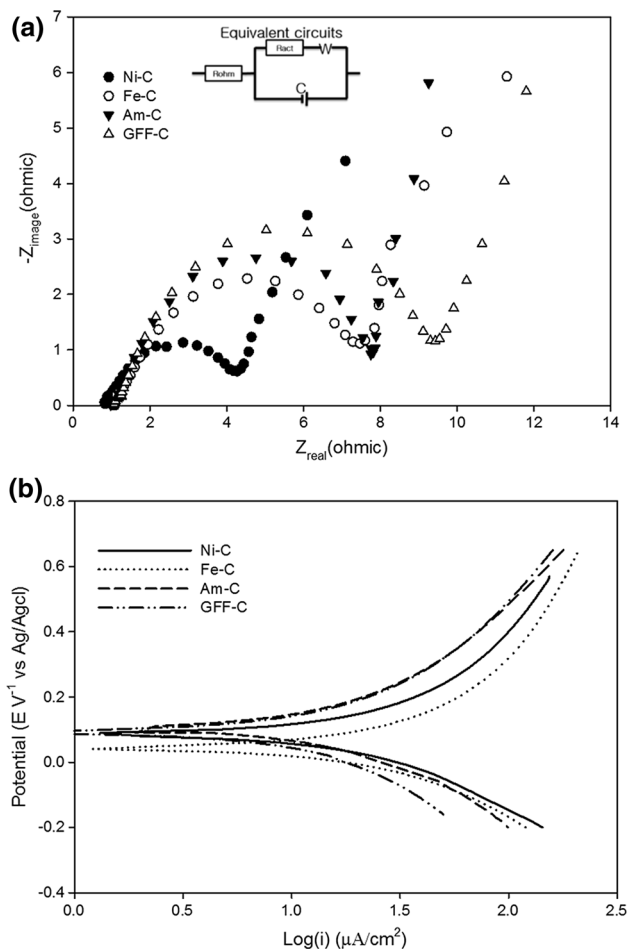

Fig. 5 a Nyquist plot of EIS data, **b** Tafel plot for the cathodes decorated with different materials

Table 3 The parameters of the EIS analysis result for different cathodes

Parameter	Ni–C	Fe–C	Am–C	GFF-C
R_s (Ω)	1.33	1.24	1.24	1.27
R_{ct} (Ω)	3.10	5.60	5.56	8.60
C (mF)	59.4	32.5	29.2	18.1
W (1 Ω^{-1} Hz^{-1})	0.223	0.356	0.406	0.482
β_c (mV dec^{-1})	−322.6	−362.6	−409.1	−474.2
i_0 (mA)	35.10	31.44	29.03	23.06

transfer of EAB on the cathode for the bioelectrochemical conversion of carbon dioxide into methane [18]. The Tafel plot for the cathodes decorated with different materials provides more information regarding the methane production from the reduction of carbon dioxide (Fig. 5b). Commonly, a smaller activation energy for an electrochemical reaction is obtained from an electrode with a smaller Tafel slope and higher exchange current [18, 49]. The Tafel slope for the Ni-C cathode was the smallest at −322.6 mV dec^{-1},

followed by Fe–C (-362.6mV dec^{-1}), and Am–C ($-409.1 \text{ mV dec}^{-1}$) (Table 3).The Tafel slope of GFF-C was the greatest as $-474.2 \text{ mV dec}^{-1}$, which was higher than those of the cathodes decorated with electron transfer assisting materials. For the exchange current, the Ni–C also obtained the greatest value of 35.10 mA, which indicates Ni is a better decoration material for bioelectrochemical methane production by assisting the electron transfer of EAB. The exchange current of Fe–C is 31.44 mA, which is similar to the 29.03 mA of Am–C, and the smallest of GFF-C is 23.06 mA. This indicates that the bioelectrochemical conversion of carbon dioxide into methane is catalyzed by Ni, Fe, and ammonia and the GFF decorated with Ni and MWCNT is the best cathode for the bioelectrochemical production of methane.

4 Conclusions

The GFF surface is well decorated with an electron transfer assisting material (Ni, Fe, or ammonia) together with MWCNT by the EPD method. The MWCNT loaded on the graphite fiber acts as an electrical bridge between graphite fibers. The decorations of MWCNT together with Ni, Fe, and ammonia considerably improve electrochemical properties of the GFF cathode. However, the decorated cathode with improved electrochemical properties requires a longer lag time for enrichment of EAB on the surface. Ni loaded on the GFF cathode considerably reduces the charge transfer resistance for the bioelectrochemical reduction of carbon dioxide on the cathode, followed by the Fe-loaded GFF cathode, and finally, the ammonia. The decoration of MWCNT together with Ni on the cathode significantly improves the bioelectrochemical production of methane, as well as, the methane yield. The benefits of this material were then followed by the decoration of Fe and ammonia.

References

1. Song YC, Kwon SJ, Woo JH (2004) Mesophilic and thermophilic temperature co-phase anaerobic digestion compared with single-stage mesophilic-and thermophilic digestion of sewage sludge. Water Res 38:1653–1662. doi:10.1016/j.watres.2003.12.019

2. Song YC, Feng Q, Ahn Y (2016) Performance of the bio-electrochemical anaerobic digestion of sewage sludge at different hydraulic retention times. Energ Fuel 30:352–359. doi:10.1021/acs.energyfuels.5b02003

3. Shin HS, Song YC (1995) A model for evaluation of anaerobic degradation characteristics of organic waste: focusing on kinetics, rate-limiting step. Environ Technol 16:775–784. doi:10.1080/09593331608616316

4. Cheng S, Xing D, Call DF, Logan BE (2009) Direct biological conversion of electrical current into methane by electromethanogenesis. Environ Sci Technol 43:3953–3958. doi:10.1021/es803531g

5. Villano M, Aulenta F, Ciucci C, Ferri T, Giuliano A, Majone M (2010) Bioelectrochemical reduction of CO_2 to CH_4 via direct and indirect extracellular electron transfer by a hydrogenophilic methanogenic culture. Bioresour Technol 101:3085–3090. doi:10.1016/j.biortech.2009.12.077

6. Guo X, Liu J, Xiao B (2013) Bioelectrochemical enhancement of hydrogen and methane production from the anaerobic digestion of sewage sludge in single-chamber membrane-free microbial electrolysis cells. Int J Hydrogen Energ 38:1342–1347. doi:10.1016/j.ijhydene.2012.11.087

7. Feng Y, Zhang Y, Chen S, Quan X (2015) Enhanced production of methane from waste activated sludge by the combination of high-solid anaerobic digestion and microbial electrolysis cell with iron–graphite electrode. Chem Eng J 259:787–794. doi:10.1016/j.cej.2014.08.048

8. Sun R, Zhou A, Jia J, Liang Q, Liu Q, Xing D, Ren N (2015) Characterization of methane production and microbial community shifts during waste activated sludge degradation in microbial electrolysis cells. Bioresour Technol 175:68–74. doi:10.1016/j.biortech.2014.10.052

9. Sasaki D, Sasaki K, Watanabe A, Morita M, Matsumoto N, Igarashi Y, Ohmura N (2013) Operation of a cylindrical bioelectrochemical reactor containing carbon fiber fabric for efficient methane fermentation from thickened sewage sludge. Bioresour Technol 129:366–373. doi:10.1016/j.biortech.2012.11.048

10. Wang A, Liu W, Cheng S, Xing D, Zhou J, Logan BE (2009) Source of methane and methods to control its formation in single chamber microbial electrolysis cells. Int J Hydrogen Energ 34:3653–3658. doi:10.1016/j.ijhydene.2009.03.005

11. Villano M, Monaco G, Aulenta F, Majone M (2011) Electrochemically assisted methane production in a biofilm reactor. J Power Sources 196:9467–9472. doi:10.1016/j.jpowsour.2011.07.016

12. Feng Q, Song YC, Bae BU (2016) Influence of applied voltage on the performance of bioelectrochemical anaerobic digestion of sewage sludge and planktonic microbial communities at ambient temperature. Bioresour Technol 220:500–508. doi:10.1016/j.biortech.2016.08.085

13. Biffinger J, Ribbens M, Ringeisen B, Pietron J, Finkel S, Nealson K (2009) Characterization of electrochemically active bacteria utilizing a high-throughput voltage-based screening assay. Biotechnol Bioeng 102:436–444. doi:10.1002/bit.22072

14. Nam JY, Tokash JC, Logan BE (2011) Comparison of microbial electrolysis cells operated with added voltage or by setting the anode potential. Int J Hydrogen energ 36:10550–10556. doi:10.1016/j.ijhydene.2011.05.148

15. Xafenias N, Mapelli V (2014) Performance and bacterial enrichment of bioelectrochemical systems during methane and acetate production. Int J Hydrogen energ 39:21864–21875. doi:10.1016/j.ijhydene.2014.05.038

16. Jiang Y, Su M, Zhang Y, Zhan G, Tao Y, Li D (2013) Bioelectrochemical systems for simultaneously production of methane and acetate from carbon dioxide at relatively high rate. Int J Hydrogen energ 38:3497–3502. doi:10.1016/j.ijhydene.2012.12.107

17. Song YC, Kim DS, Woo JH, Subha B, Jang S, Sivakumar S (2015) Effect of surface modification of anode with surfactant on the performance of microbial fuel cell. Int J Energ Res 39:860–868. doi:10.1002/er.3284

18. Feng Q, Song YC (2016) Surface modification of a graphite fiber fabric anode for enhanced bioelectrochemical methane

production. Energ Fuel 30:6467–6474. doi:10.1021/acs.energy fuels.6b00959

19. Tsai HY, Wu CC, Lee CY, Shih EP (2009) Microbial fuel cell performance of multiwall carbon nanotubes on carbon cloth as electrodes. J Power Sources 194:199–205. doi:10.1016/j.jpow sour.2009.05.018

20. Deng Q, Li X, Zuo J, Ling A, Logan BE (2010) Power generation using an activated carbon fiber felt cathode in an upflow microbial fuel cell. J Power Sources 195:1130–1135. doi:10.1016/j.jpowsour.2009.08.092

21. Wei J, Liang P, Huang X (2011) Recent progress in electrodes for microbial fuel cells. Bioresour Technol 102:9335–9344. doi:10.1016/j.biortech.2011.07.019

22. Zhou M, Chi M, Luo J, He H, Jin T (2011) An overview of electrode materials in microbial fuel cells. J Power Sources 196:4427–4435. doi:10.1016/j.jpowsour.2011.01.012

23. Kadier A, Simayi Y, Chandrasekhar K, Ismail M, Kalil MS (2015) Hydrogen gas production with an electroformed Ni mesh cathode catalysts in a single-chamber microbial electrolysis cell (MEC). Int J Hydrogen Energy 40(41):14095–14103. doi:10.1016/j.ijhydene.2015.08.095

24. Dai H, Yang H, Liu X, Jian X, Liang Z (2016) Electrochemical evaluation of nano-Mg(OH)$_2$/graphene as a catalyst for hydrogen evolution in microbial electrolysis cell. Fuel 174:251–256. doi:10.1016/j.fuel.2016.02.013

25. Chen Y, Xu Y, Chen L, Li P, Zhu S, Shen S (2015) Microbial electrolysis cells with polyaniline/multi-walled carbon nanotube-modified biocathodes. Energy 88:377–384. doi:10.1016/j.energy.2015.05.057

26. Wang Y, Fang B, Li H, Bi XT, Wang H (2016) Progress in modified carbon support materials for Pt and Pt-alloy cathode catalysts in polymer electrolyte membrane fuel cells. Prog Mater Sci 82:445–498. doi:10.1016/j.pmatsci.2016.06.002

27. Oliveira V, Simões M, Melo L, Pinto A (2013) Overview on the developments of microbial fuel cells. Biochem Eng J 73:53–64. doi:10.1016/j.bej.2013.01.012

28. Watson VJ, Delgado CN, Logan BE (2013) Improvement of activated carbons as oxygen reduction catalysts in neutral solutions by ammonia gas treatment and their performance in microbial fuel cells. J Power Sources 242:756–761. doi:10.1016/j.jpowsour.2013.05.135

29. Singh S, Verma N (2015) Graphitic carbon micronanofibers asymmetrically dispersed with alumina-nickel nanoparticles: a novel electrode for mediatorless microbial fuel cells. Int J Hydrogen Energ 40:5928–5938. doi:10.1016/j.ijhydene.2015.03.010

30. Yen SJ, Tsai MC, Wang ZC, Peng HL, Tsai CH, Yew TR (2013) The improvement of catalytic efficiency by optimizing Pt on carbon cloth as a cathode of a microbial fuel cell. Electrochim Acta 108:241–247. doi:10.1016/j.electacta.2013.06.019

31. Ando T, Izhar S, Tominaga H, Nagai M (2009) Ammonia-treated carbon-supported cobalt tungsten as fuel cell cathode catalyst. Electrochim Acta 55(8):2614–2621. doi:10.1016/j.electacta.2009.12.039

32. Liu G, Li X, Ganesan P, Popov BN (2010) Studies of oxygen reduction reaction active sites and stability of nitrogen-modified carbon composite catalysts for PEM fuel cells. Electrochim Acta 55(8):2853–2858. doi:10.1016/j.electacta.2009.12.055

33. Siegert M, Yates MD, Call DF, Zhu X, Spromann A, Logan BE (2014) Comparison of nonprecious metal cathode materials for methane production by electromethanogenesis. ACS Sustainable Chem Eng 2(4):910–917. doi:10.1021/sc400520x

34. Sangeetha T, Guo Z, Liu W, Cui M, Yang C, Wang L, Wang A (2016) Cathode material as an influencing factor on beer wastewater treatment and methane production in a novel integrated upflow microbial electrolysis cell (Upflow-MEC). Int J Hydrogen Energ 41(4):2189–2196. doi:10.1016/j.ijhydene.2015.11.111

35. Cheng S, Logan BE (2007) Ammonia treatment of carbon cloth anodes to enhance power generation of microbial fuel cells. Electrochem Commun 9:492–496. doi:10.1016/j.elecom.2006.10.023

36. Ullery ML, Logan BE (2015) Anode acclimation methods and their impact on microbial electrolysis cells treating fermentation effluent. Int J Hydrogen Energ 40:6782–6791. doi:10.1016/j.ijhydene.2015.03.101

37. Kim DH, Song YC, Feng Q (2015) Influence of applied voltage for bioelectrochemical anaerobic digestion of sewage sludge. J Korean Soc Environ Eng 37:542–549. doi:10.4491/KSEE.2015.37.9.542

38. Woo JH, Song YC (2010) Influence of temperature and duration of heat treatment used for anaerobic seed sludge on biohydrogen fermentation. KSCE J Civ Eng 14:141–147. doi:10.1007/s12205-010-0141-5

39. Kim KS, Park SJ (2012) Bridge effect of carbon nanotubes on the electrical properties of expanded graphite/poly (ethylene terephthalate) nanocomposites. Carbon Lett 13:51–55. doi:10.5714/CL.2012.13.1.051

40. Kalakonda P, Cabrera Y, Judith R, Georgiev GY, Cebe P, Iannacchione GS (2015) Studies of electrical and thermal conductivities of sheared multi-walled carbon nanotube with isotactic polypropylene polymer composites. Nanomater Nanotechnol 5:2. doi:10.5772/60083

41. Parot S, Délia M-L, Bergel A (2008) Forming electrochemically active biofilms from garden compost under chronoamperometry. Bioresour Technol 99:4809–4816. doi:10.1016/j.biortech.2007.09.047

42. Rolfe MD, Rice CJ, Lucchini S, Pin C, Thompson A, Cameron AD et al (2012) Lag phase is a distinct growth phase that prepares bacteria for exponential growth and involves transient metal accumulation. J Bacteriol 194:686–701. doi:10.1128/JB.06112-11

43. Yoon SM, Choi CH, Kim M, Hyun MS, Shin SH, Yi DH, Kim HJ (2007) Enrichment of electrochemically active bacteria using a three-electrode electrochemical cell. J Microbiol Biotechnol 17:110–115

44. Cercado B, Cházaro-Ruiz LF, Ruiz V, López-Prieto LDJ, Buitrón G, Razo-Flores E (2013) Biotic and abiotic characterization of bioanodes formed on oxidized carbon electrodes as a basis to predict their performance. Biosens Bioelectron 50:373–381. doi:10.1016/j.bios.2013.06.051

45. Cheng Q, Chen Z (2013) The cause analysis of the incomplete semi-circle observed in high frequency region of EIS obtained from TEL-covered pure copper. Int J Electrochem Sci 8:8282–8290

46. Quintero OMS, Chaparro WA, Ipaz L, Barco JES, Beltrán FE, Zambrano G (2013) Influence of the microstructure on the electrochemical properties of Al–Cr–N coatings deposited by co-sputtering method from a Cr–Al binary target. Mater Res 16:204–214. doi:10.1590/S1516-14392012005000171

47. Yamada Y, Iriyama Y, Abe T, Ogumi Z (2010) Kinetics of electrochemical insertion and extraction of lithium ion at SiO. J Electrochem Soc 157:A26–A30. doi:10.1149/1.3247598

48. Ishihara Y, Miyazaki K, Fukutsuka T, Abe T (2014) Kinetics of lithium-ion transfer at the interface between Li4Ti5O12 thin films and organic electrolytes. ECS Electrochem Lett 3:A83–A86. doi:10.1149/2.0011408eel

49. Feng Q, Song YC, Yoo K, Lal B, Kuppanan N, Subudhi S, Choi TS (2016) Performance of upflow anaerobic bioelectrochemical reactor compared to the sludge blanket reactor for acidic distillery wastewater treatment. J Korean Soc Environ Eng 38(6):279–290. doi:10.4491/KSEE.2016.38.6.279